Published in final edited form as:
J Biol Inorg Chem. 2014 June ; 19(0): 555–563. doi:10.1007/s00775-013-1077-2.

A Euclidean Perspective on the Unfolding of Azurin: Chain Motion

Harry B. Gray[†], **Jeffery J. Warren**[†,§], **Jay R. Winkler**[†], and **John J. Kozak**[‡]
John J. Kozak: kozak@depaul.edu
[†]Beckman Institute, California Institute of Technology, Pasadena, CA 91125, USA
[‡]Department of Chemistry, DePaul University, 243 South Wabash Avenue, Chicago, IL 60660-8875, USA

Abstract

We present a new approach to visualizing and quantifying the displacement of segments of *P. aeruginosa* azurin in the early stages of denaturation. Our method is based on a geometrical method developed previously by the authors, and elaborated extensively for azurin. In this study, we quantify directional changes in three α-helical regions, two regions having β-strand residues, and three unstructured regions of azurin. Snapshots of these changes as the protein unfolds are displayed and described quantitatively by introducing a scaling diagnostic. In accord with MD simulations, we show that the long α-helix in azurin (residues 54–67) is displaced from the polypeptide scaffolding and then pivots first in one direction, and then in the opposite direction as the protein continues to unfold. The two β-strand chains remain essentially intact and, except in the earliest stages, move in tandem. We show that unstructured regions 72–81 and 84–91, hinged by β-strand residues 82–83, pivot oppositely. The region comprised of residues 72–91 (40% hydrophobic and 16% of the 128 total residues), forms an effectively stationary region that persists as the protein unfolds. This *static* behavior is a consequence of a dynamic balance between the competing motion of two segments, residues 72–81 and 84–91.

Keywords

protein folding; azurin; modeling

I. Introduction

Since the pioneering work of van der Waals in the 19th century, it has been recognized that repulsive forces, and attendant excluded volume effects, play the dominant role in defining the structure of the liquid state [1–4]. In the study of protein structure, the role of excluded volume was emphasized in the seminal contributions of Ramachandran and co-workers

Correspondence to: John J. Kozak, kozak@depaul.edu.
[§]Current Address: Simon Fraser University, Department of Chemistry, 8888 University Drive, Burnaby BC V5A 1S6, Canada j.warren@sfu.ca

Supplementary Material
Example calculation of S_i and β_i, expanded version of Figure 4, coordinates for all unfolding cases studied. Supplementary Material is available online.

(e.g., [5]). The native state of a protein represents an optimized and sensitive balance between excluded volume effects and both short- and long-range attractions between and among the constituent residues. In previous work, we explored the consequences of relaxing steric constraints in the early stages of denaturation. We focused on *Pseudomonas aeruginosa* azurin (Figure 1) and documented changes in the spatial coordinates of each residue with respect to the Cu^{2+} ion [6]. We then extended our model to quantify the associated changes in the angular configuration of neighboring residues as the protein unfolds [7]. In the present study, we further develop our geometrical approach to track the motion of distinct regions of the polypeptide chain as azurin denatures; we consider α-helical regions, β-strand residues, and regions in which secondary structure is absent.

In Section II.a we briefly review our geometrical approach and introduce a generalization, which allows us to construct snapshots of the relative motion of segments of the polypeptide chain in the early stages of denaturation. In Section II.b these representations are supplemented by a diagnostic, which allows a quantitative description of chain motion. Results, discussion and conclusions are presented in Section III–V, respectively.

II. Methods

II.a Segment Motion

Our geometrical model presented for azurin [6,7], and elaborated previously for several other proteins [8–10], makes fundamental use of crystallographic data for each protein being studied. From these data, the geometry of n = 3 residues, a central residue and its two nearest-neighbors, is determined for each residue of the polypeptide chain (except the two terminal ones). The geometry of each triplet is maintained invariant in all subsequent calculations. The early stages of unfolding are represented by relaxing, sequentially, the native state geometry of segments of n = 5, 7, 9, and so on, up to 15 residues of the polypeptide chain. Among the possible relaxed conformations that could, in principle, be realized, we specify the fully unfolded state to be represented by a linear sequence of native state triplets. For example, for azurin in the n = 5 unfolded state, the sequence of five residues, Ser34, His35, Pro36, Gly37, and Asn38, is represented by two triplets, Ser34-His35-Pro36 and Pro36-Gly37-Asn38, centered on Pro and aligned in a linear array. The stage n = 7 is specified by three triplets in a linear array, n = 9 by four triplets, and so on, up to n = 15 with seven triplets in a linear array.

At each stage of unfolding, the length of the sides and the defining angles of the triangle formed by connecting the left-most and right-most residue in a segment to the Cu^{2+} are determined (see [6,7] for full details). The distances and angles characterizing, for example, the triangle Ser34-Cu-Asn38, are specified with respect to the coordinates of the Cu and the calculated coordinates of the α-carbon of Ser34 and Asn38. This calculation is done for each internal residue for each stage of unfolding of the protein. The results obtained are used to quantify the relaxation of spatial and angular correlations as azurin denatures. Once the geometrical model is defined, all subsequent calculations are carried out without introducing *any* further approximations.

As elaborated in Ref. [7], insights on the torsional motion of the unfolding polypeptide chain can be inferred from changes in a defined, angular signature Δ. By construction, if the triangle formed among three residues is perfectly isosceles, the signature is Δ = 0. Values of Δ greater or less than zero specify the degree to which the triangle is scalene.

From tabulations of the signature Δ, we confirmed that on denaturation the predicted directional change in motion of the extended α-helix in azurin (residues 54–67) was in substantial agreement with results obtained in the molecular dynamics (MD) simulations of Rizzuti *et al*. [11]. In what follows, we introduce a direct (as opposed to inferential) method of characterizing the motion all regions of the polypeptide chain as the protein unfolds.

To proceed, consider the sequence of residues: Ser34, His35, Pro36, Gly37, and Asn38. The distance of each of these residues from the Cu in the native state and the distance between any pair of residues are readily calculated from crystallographic data [12]. Using the geometrical methods introduced in Refs. [6–9], the distance of each of these residues from the Cu^{2+} in the first *unfolded* state (n = 5) also can be calculated, as can the distance between any pair of residues. For the above sequence of five residues, we now construct three triangles (Figure 2) Ser34-His35-Pro36 (red), His35-Pro36-Gly37 (blue), and Pro36-Gly37-Asn38 (green). The length of each side and the angles of the vertices of these triangles can be determined exactly for the native state and for the unfolded states [6,7].

In the spirit of Kadanoff's "block-spin" renormalization group theory [13,14], wherein a system in which atoms (spins) interact only with nearest neighbors is divided into blocks, and block variables are introduced to describe the average behavior of the block, we now replace the three triangles in Fig. 2, by a single, encompassing "block" triangle, Ser34-Pro36-Asn38 (vertices shown in bold in Fig 2). Figure 3 illustrates the evolution of these block triangles for the native state through n =15. Comparison of the native and n = 5 triangles in Fig. 3 shows that the left-most vertex (Ser34) remains essentially stationary when the native state begins to unfold, whereas there is a noticeable shift in the position of the right-most residue (Asn38). This behavior may be described qualitatively by saying that the overall configuration of constituent residues (Ser34-His35-Pro36-Gly37-Asn38) pivots clockwise with respect to Cu as the protein unfolds from the native to n = 5 state.

II.b A Quantitative Diagnostic

We now introduce a quantitative diagnostic to document the pivoting behavior illustrated in Fig. 3 for any sequence of residues in the polypeptide chain (Fig. 1). In Ref. [6], the distance of each residue i from the Cu^{2+} was calculated for the native-state geometry and for the extended-states (n = 3–15). From these data, a spatial signature $\mathbf{S_i}$ for each residue i at each stage was defined as the ratio of the calculated distance in the extended state to the distance in the native state. By construction, the value $\mathbf{S_i} = 1$ defines the native state, and values of $\mathbf{S_i}$ different from unity calibrate the spatial displacement of each residue at a given stage of unfolding relative to the native state. Likewise, the angular signature ($\boldsymbol{\beta_i}$) [7] is the ratio of the angle formed by the left-most residue (lowest residue number) and right-most residue (highest residue number) in a given extended state, and the angle for the same three residues in the native state (see Supporting Information).

In the example illustrated in Figs. 1 and 2, the net displacement of residue Ser34 relative to the native state is specified by

$$\tau_{\mathrm{L}}=\mathrm{S_i(i=34)}-1 \quad (1)$$

and the net displacement of residue 38 relative to the native state by

$$\tau_{\mathrm{R}}=\mathrm{S_i(i=38)}-1 \quad (2)$$

The ratio of τ_{L} to τ_{R} is designated:

$$\mathrm{T(36)}=\tau_{\mathrm{L}}/\tau_{\mathrm{R}} \quad (3)$$

The more pronounced displacement of the right-most residue of the “block” triangle, Ser34-Pro36-Asn38, for the n = 5 unfolded state (Fig. 3, red) relative to the native state (Fig. 3, gray) is characterized by a value T < 1. A value of T > 1 signals that the more pronounced displacement is toward the left-most residue Ser34. For segments of increasing length centered on the residue Pro36, values of τ_{L}, τ_{R} and T can be calculated for each stage of unfolding, n = 5 through n = 15. A similar program has been carried out for several of the key features of azurin (see below). We will use the diagnostic T to track motional changes of extended segments of the polypeptide chain as azurin denatures.

III. Results

The portions of azurin considered in this study are shown in Fig. 1: residues in the long α-helical region (H2: 54–67) in blue, shorter α-helical regions (H1: 40–45 and H3: 116–120) in green, β-strand regions (S1: 28–34 and S2: 92–98) in red, and unstructured regions (K1: 9–18, K2A: 72–81 and K2B: 84–91) in orange. Note that in our earlier work we differentiated between internal residues in a given α-helix versus those at the “interface” between regions. For simplicity here, we adopt here the regions of α−helical and β-strand residues specified in the crystallographic study of Crane *et al*. (PDB ID 1JZF, [12]), with one exception: in order to make direct comparison with MD simulations [11], we designate the boundary residues for the long α-helical region as 54–67, rather than 55–65 as [12].

Using previously calculated signatures, S_i, β_i, and Δ_i [6,7], we have determined overall averages for the regions shown in Fig. 1. Note that region K2 is the aggregate region that encompasses K2A and K2B. These averages were determined by calculating the area under the curve generated when a given signature is plotted as a function of residue number for stage n, normalized by the value calculated for the native state. The region averages for S_i are given in Table 1, for β_i in Table 2, and for Δ_i in Table 3.

The data in Table 4 record the corresponding region averages for τ_{L}, τ_{R} and their ratio T. The directional change of regions of the polypeptide chain can be followed as the protein unfolds using these data. For example, consider the primary α-helical region H2 (residues 54–67). As inferred from our analysis of the signature Δ_i [7], but evident from the data presented in Table 4, the helix H2 pivots first one way, then reverses direction as azurin denatures, in full agreement with MD simulations [11]. It is important point out that the

direction of rotation depends on the choice of the origin for the coordinate system. The quantitative metrics will change accordingly, but the qualitative behavior of the protein structures does not depend on the choice of origin.

In order to fashion a more global picture of the unfolding of azurin, region by region, we present composite pictures of the position of the α-carbons (Figure 4). The overall motion of a defined segment of the polypeptide chain in the first, n = 5 stage of unfolding is determined by constructing the average <T> of the set of T_i for each residue i comprising that region normalized with respect to the native state. If the net displacement of the left-most member of that segment is more pronounced than the right-most member, the segment is shown in cyan; if the more pronounced displacement is in the opposite direction, the segment is shown in magenta. Other color coding is as in Fig. 1.

IV. Discussion

IV.1 Quantifying early stages of azurin unfolding

We elaborated a novel way of visualizing and quantifying the displacements of α-helical, β-strand and unstructured segments of azurin upon initial denaturation. While our principal focus is on the unfolding of azurin, folded proteins exhibit a variety of fluctuations, so the results presented here for early stages of denaturation give insight on the resiliency of the native structure to steric perturbations. Our conclusions follow from the summary portraits of the motional behavior of these regions, presented in Figure 5, where we plot the ratio $T = \tau_L/\tau_R$ for the several extended regions considered in this study.

In Fig. 5a the profile of T versus the extension index n is displayed for the three α - helical regions H1, H2 and H3. Both the helix H1 and the helix H3 comprising show a pronounced counterclockwise motion, followed by a pronounced clockwise motion. Qualitatively similar behavior was found for the extended α-helix H2, although here motional changes are suppressed and the reversal much more gradual. The crossover for all three helices is in the vicinity of a segment length n = 9. Since each turn of the α-helix requires 3.6 residues, both H1 (with six residues) and H3 (with five residues) are effectively one-turn helices; the helix H2 (with 13 residues) will have three turns. The more lethargic response of the helix H2 as steric constraints are relaxed probably reflects the enhanced cooperativity of residues comprising the extended secondary structure of this region.

As shown in Figures 4 and 5, residues comprising the β-strand regions S1 and S2 remain essentially intact during the early stages of denaturation. The pivoting behavior of region S2 is similar to the behavior of helical region (H3). The pivoting behavior of region S1 is consistently clockwise. Except in the earliest stage of unfolding, the displacements of β-regions S1 and S2 are in tandem though motional changes for S1 are more suppressed.

The behavior of the unstructured region K1, is similar to that of helices H1 and H3, although the crossover point shifts from n = 9 to n = 11. This delay is probably a consequence of the greater number of residues in region K1 versus regions H1 and H3 (10 versus 6 and 5). In the early stages of unfolding region K2A is displaced in one direction, and region K2B in the opposite direction. The composite region (K2), containing both K2A and K2B, remains

essentially immobile as azurin unfolds. We suggest that the effective, stationary behavior exhibited by the polypeptide segment K2 is the consequence of dynamic tension, a "standoff" between opposing motions of two constituent segments K2A and K2B. During the folding of azurin, a core hydrophobic region serves as a nucleus for self-assembly. The region K2 is comprised, overall, of 20 residues, about 16% of the total number in azurin (128). Of the 20 residues, eight (~40%) are definitely hydrophobic. Although this is not the prototypical hydrophobic core [15], it displays noteworthy stability that is a result of dynamic motions in two halves of the overall region.

Finally, we again draw attention to the studies of Guzzi and coworkers [11,16–20] in which they emphasize the importance of Trp48 as "a natural probe to verify the exposure of the hydrophobic core." Since Trp48 is well buried in the core of azurin, and fluorescence can be used as a sensitive probe of the integrity of the protein fold. They found that the core of the protein is stable during initial unfolding, but once helix H2 is displaced from the scaffolding of azurin, Trp48 becomes exposed to solvent. Their experimental evidence showed that the exposure to the solvent of Trp48 "preceded not only the melting of much of the secondary structure but also the complete disruption of the tertiary structure."

We previously [6] calculated the displacement of most of the residues of azurin relative to Cu^{2+} as the protein unfolded, and constructed a spatial signature $\mathbf{S_i}$, the ratio of the distance (of the α-carbon) of a given residue in the extended state (n) to the native state. The signature $\mathbf{S_i}$ for Trp48 changed from 1.00 in the native state to 1.04 in stage n = 5, 1.05 in n = 7, 1.12 in n = 9, 1.24 in n = 11, 1.39 in n = 13 and 1.77 in n = 15. Translated into Å, the distance of the α-carbon of Trp48 from Cu^{2+} in the native state, 8.3 Å, changes on unfolding to 8.6, 8.7, 9.3, 10.3, 11.5, and 14.7 Å for n = 3 to 15, respectively. As seen from Table 1, these changes are comparable to (overall) changes in S1 and S2, the regions comprised of β-strand residues.

Our calculations show that changes in the (average) signature $\langle S_i \rangle$ are most pronounced for the α-helical regions, H1, H2, and H3, less so for the dynamic K2, and certainly greater than for the regions S1 and S2, in accord with the principal conclusions in [11] and the earlier MD study of Arcangeli *et al*. [21]. We also find that changes in the position of the residue Trp48 relative to Cu^{2+} in the early stages of denaturation are, like the β-strand regions S1 and S2, of the order of an Ångstrom (see above), noticeably smaller than that of the hydrophobic core K2 or the α-helical regions. This behavior is in agreement with the MD simulations in Ref. (8).

IV.2 Comments on the geometrical approach

Ramachandran's seminal work identified the role of excluded-volume effects in restricting native state protein configurations. These accessible configurations are identified via a plot of the backbone dihedral angles ϕ and ψ of the constituent residues [5]. Our geometrical approach proceeds by a segment-by-segment analysis of the unfolding of the crystallographically defined native structure, which can be regarded as describing the "melting" of regions defined by the [ϕ, ψ] plot. The significant new feature introduced here is that we quantitatively characterize configuration changes in the native structure as the protein unfolds. While our model is not designed to capture the same dynamic features as

high-level simulations, we arrive at many of the same conclusions regarding bulk motions of important protein segments. This suggests that our approach could be a simple starting point for refining the specific focus of high-level computational approaches in complicated protein systems. The following paragraphs highlight the underlying physical features of our model and contrast it to advanced simulations.

To provide physical insight on why our geometrical model is able to capture and characterize the local stability of azurin, as well as the other proteins [8–10], we take advantage of results drawn from the theory of classical fluids [1–4]. In these theories, repulsive (geometrical) forces between the molecules comprising a dense fluid are the primary determinant of liquid structure. Excluded-volume effects arising from repulsive interactions also govern the transition between liquid and the solid states. Attractive interactions are thought to “fine tune” the interactions between molecules in a fluid, leading to the thermodynamic differences found experimentally among different molecular systems. In addition, the liquid-gas transition and critical phenomena are driven by long-range attractive interactions. This characterization of the factors influencing the stability of phases was shown to follow from a rigorous analysis of equations derived from the distribution function theory of liquids for a system of rigid spheres of diameter σ surrounded by an attractive core of strength ε, which extends to separations $R\sigma$ [22].

In our approach, we argue that unfolding of a protein from native to disordered configurations is conceptually similar to the disruption of a solid to a liquid, a quasi-random system with *local* structure determined *primarily* by short-range correlations. The geometric model introduced here gives a systematic way of following the local relaxation of steric constraints between and among segments of the polypeptide chain as the protein unfolds. It is important to stress that the success of our approach is predicated on a high-fidelity (optimized) starting point, i.e., the crystallographic structure.

Our model involves only theorems from plane geometry and trigonometry, so it is computationally inexpensive. Once translated into a program, the compilation times required to execute the calculation on a standard desktop computer are vanishingly small compared to full-scale MD simulations, the most sophisticated of which are carried out on supercomputers. Beyond this calculation aspect, a further advantage of our model is that the unfolding of the protein can be followed to a greater degree of denaturation, corresponding to longer times. The best MD simulations follow unfolding to a few nanoseconds, thus capturing only the earliest stages of denaturation.

Furthermore, MD simulations often are run at higher than ambient temperatures to advance the disruption of the polypeptide chain, the assumption being that the behavior induced still portrays the behavior of the protein at lower temperatures. Our approach requires no additional assumption concerning the temperature of the system. Guided by our understanding of the solid-liquid transition in classical fluids, we argue that temperature independent excluded volume effects determine the main structural features of protein denaturation; we regard temperature dependent down-range attractive interactions as a perturbation.

V. Conclusion

We developed a comprehensive model to describe the behavior of major segments of azurin in the early stages of unfolding. While our purely geometric model cannot predict specific unfolded structures (which reflect the interplay of both short-range and long-range potential interactions), it does capture the dominant unfolding behavior of important protein structures. Our results are in excellent agreement with experiment and MD simulations, which is noteworthy since MD simulations are computationally intensive and calculations based on our geometrical (analytic) model are not. We are presently using the approach described in this study to characterize the denaturation of a range of proteins, including those studied previously [8–10].

Supplementary Material

Refer to Web version on PubMed Central for supplementary material.

Acknowledgments

Work at Caltech was supported by NIH (GM095037 to JJW and DK019038 to HBG and JRW).

References

1. Hansen, J-P.; McDonald, IR. Theory of Simple Liquids. 3rd Ed.. Amsterdam: Elsevier; 2006.
2. Hirshfelder, JO.; Curtiss, CF.; Bird, RB. Molecular Theory of Gases and Liquids. New York: John Wiley & Sons; 1954.
3. Rice, SA.; Gray, P. The Statistical Mechanics of Simple Fluids. New York: Interscience Publishers; 1965.
4. Goodstein, DL. States of Matter. New York: Dover Publications; 1985.
5. Ramachandran GN V, Sasisekharan V. Adv Protein Chem. 1968; 23:283–437. [PubMed: 4882249]
6. Warren JJ, Gray HB, Winkler JR, Kozak JJ. Mol Phys. 2013; 111:922–929. [PubMed: 23853392]
7. Warren JJ, Gray HB, Winkler JR, Kozak JJ. Mol Phys. 2013 (published online, 23 April 2013).
8. Urie KG, Pletneva E, Gray HB, Winkler JR, Kozak JJ. Mol Phys. 2010; 109:301–313. [PubMed: 21379364]
9. Gray HB, Winkler JR, Kozak JJ. Mol Phys. 2011; 110:419–429.
10. Gray HB, Winkler JR, Kozak JJ. Mol Phys. 2011; 109:905–916.
11. Rizzuti B, Daggett V, Guzzi R, Sportelli L. Biochemistry. 2004; 43:15604–15609. [PubMed: 15581373]
12. Crane BR, Di Bilio AJ, Winkler JR, Gray HB. J Am Chem Soc. 2001; 123:11623–11631. [PubMed: 11716717]
13. Kadanoff LP. Nuovo Cimento. 1966; 44:276–305.
14. Kadanoff LP. Physics. 1966; 2:263–272.
15. Wilson CJ, Wittung-Stafshede P. Proc Natl Acad Sci USA. 2005; 102:3984–3987. [PubMed: 15753320]
16. La Rosa C, Milardi D, Grasso D, Guzzi R, Sportelli L. J Phys Chem. 1995; 99:14864–14870.
17. Guzzi R, La RC, Grasso D, Milardi D, Sportelli L. Biophys Chem. 1996; 60:29–38.
18. Guzzi R, Sportelli L, La Rosa C, Milardi D, Grasso D, Verbeet MP, Canters GW. Biophys J. 1999; 77:1052–1063. [PubMed: 10423449]
19. Rizzuti B, Swart M, Sportelli L, Guzzi R. J Mol Model. 2004; 10:25–31. [PubMed: 14691672]
20. Manetto GD, Grasso DM, Milardi D, Pappalardo M, Guzzi R, Sportelli L, Verbeet MP, Canters GW, La Rosa C. ChemBioChem. 2007; 8:1941–1949. [PubMed: 17868155]

21. Arcangeli C, Bizzarri AR, Cannistraro S. Biphys Chem. 1999; 78:247–257.
22. Piasecki J, Szymczak P, Kozak JJ. J Chem Phys. 2013; 138 164506(1–11).

```
1    ALA GLU CYS SER VAL ASP ILE GLN GLY ASN ASP GLN MET GLN PHE ASN THR
                                     |-----------------K1---------------

18   ASN ALA ILE THR VAL ASP LYS SER CYS LYS GLN PHE THR VAL ASN LEU SER
     ---|                                  |-------------S1-----------|

35   HIS PRO GLY ASN LEU PRO LYS ASN VAL MET GLY HIS ASN TRP VAL LEU SER
                         |---------H1----------|

52   THR ALA ALA ASP MET GLN GLY VAL VAL THR ASP GLY MET ALA SER GLY LEU
                   |--------------------H2----------------------|

69   ASP LYS ASP TYR LEU LYS PRO ASP ASP SER ARG VAL ILE ALA HIS THR LYS
                   |-------------------K2A--------------|          |------

86   LEU ILE GLY SER GLY GLU LYS ASP SER VAL THR PHE ASP VAL SER LYS LEU
     ----K2B---------------|  |-----------S2------------|

103  LYS GLU GLY GLU GLN TYR MET PHE PHE CYS THR PHE PRO GLY HIS SER ALA
                                                       |-------H3-----

120  LEU MET LYS GLY THR LEU THR LEU LYS
     --|
```

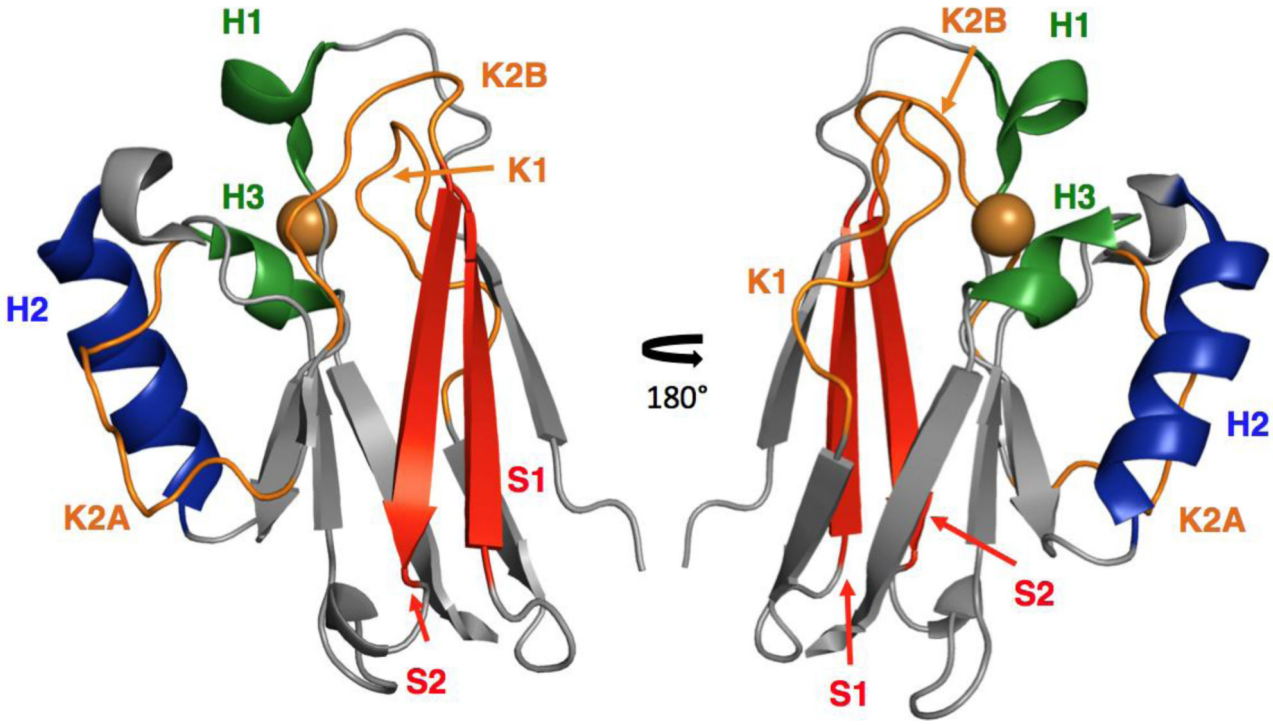

Figure 1.

Azurin sequence and segment identification. The two orientations of azurin shownb at the bottom are the same as in Figure 4.

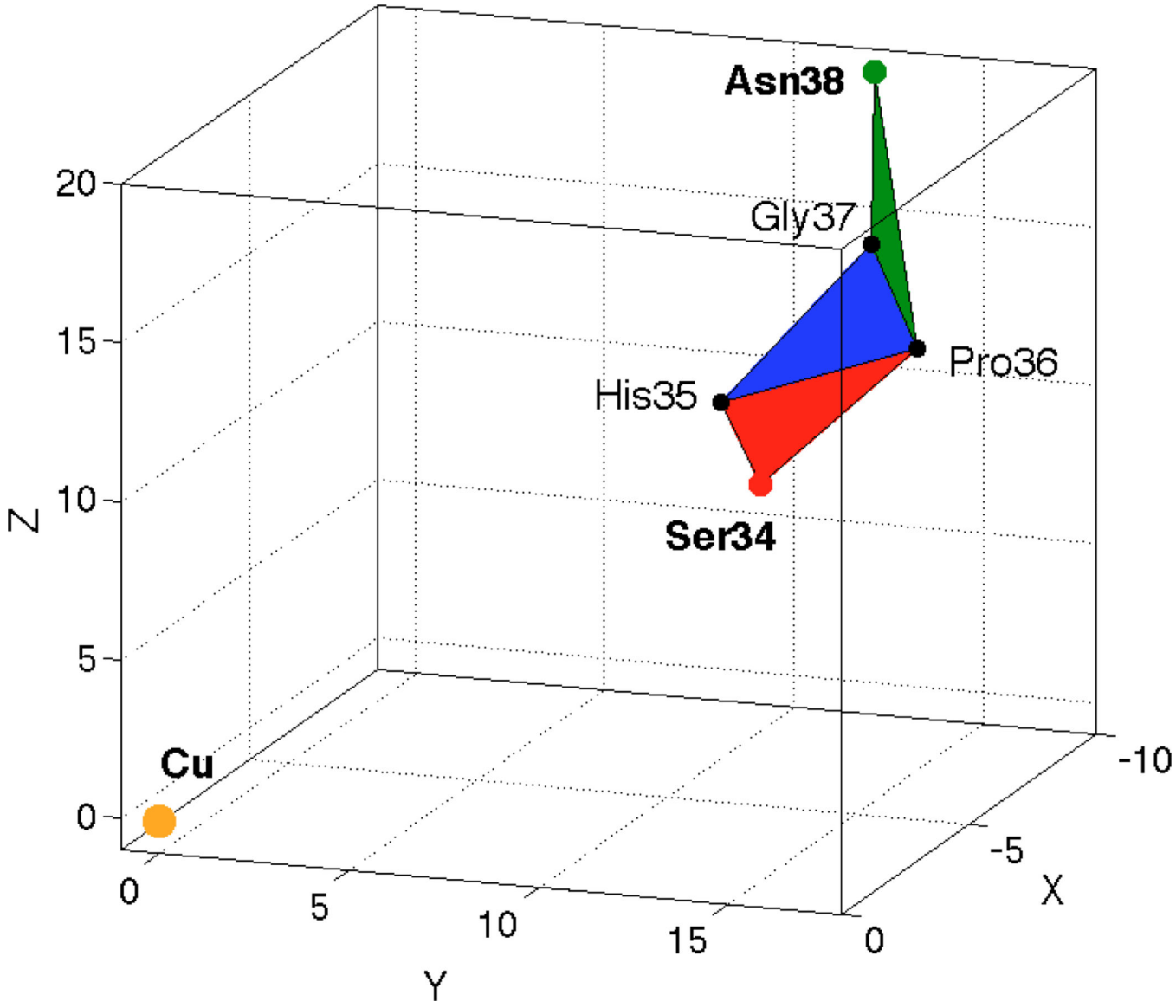

Figure 2.

The first stage of unfolding (n = 5) is shown by the red triangle connecting the α-carbons of the three residues, Ser34, His35, and Pro36. Likewise, the triangles formed by His35, Pro36, Gly37 and by Pro36, Gly37, Asn38 are shown in blue and green, respectively. A “block” triangle for n = 5 is formed by connecting Ser34, Pro36 and Asn38. The orange circle shows the location of Cu^{2+}.

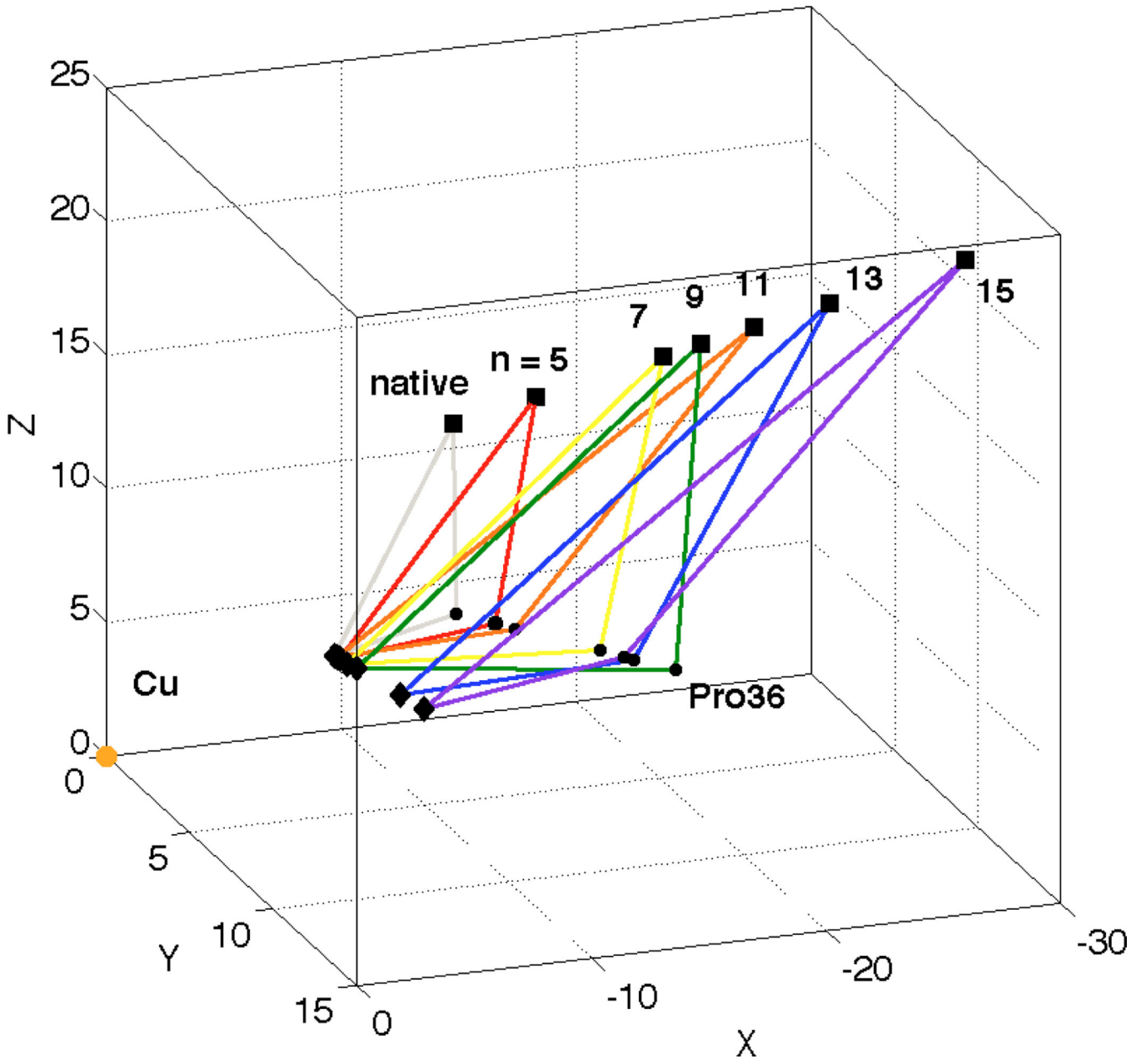

Figure 3.

"Block" triangles for the progression from n = 5 to 15 centered on Pro36. Left-most residue is shown as a diamond and the right-most residue is shown as a square. The orange circle denotes the location of Cu^{2+}.

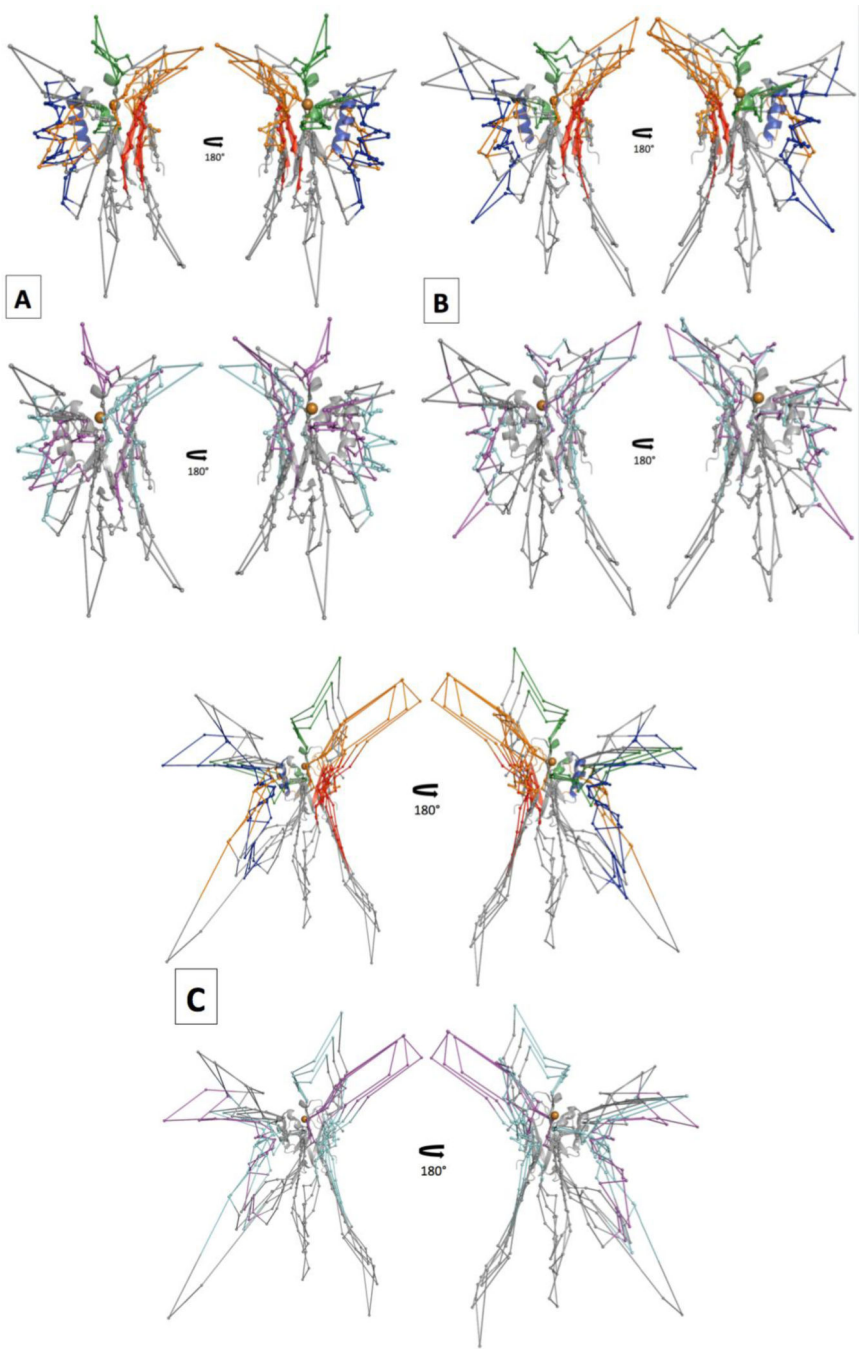

Figure 4.

Position of the α-carbons for each azurin segment for unfolding metrics (A) n = 5 and 7; (B) 7 and 9; (C) and n = 11, 13, 15. The bottom row shows polypeptide segments that pivot toward the left-most residue (cyan) or rightmost residue (magenta) of the corresponding "block" triangles. The native protein structure is shown as a semi-transparent ribbon and Cu^{2+} is shown as an orange sphere. Full-page versions of this Figure are given in the Supporting Information.

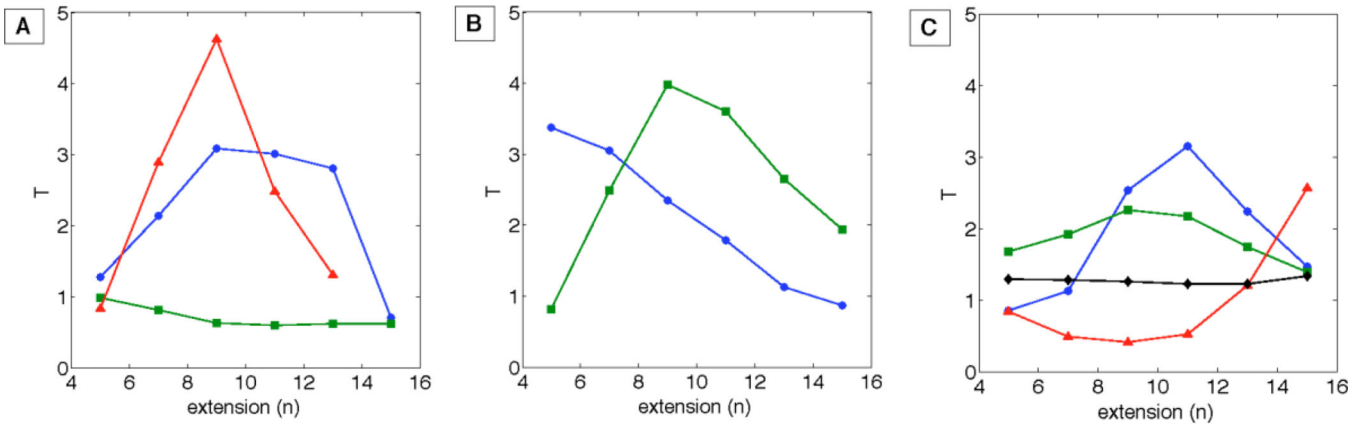

Figure 5.

The metric T versus the extension index n for: (a) the α-helical regions H_1 (blue ●), H_2 (green ■) and H_3 (red ▲); (b) the β-strand regions S_1 (blue ●) and S_2 (green ■); and (c) the four unstructured regions K1 (blue ●) K2A (green ■), K2B (red ▲) and K2 (black ♦).

Table 1

$\langle S_i \rangle$ for stages n=5 to n=15

Segment	Region	n = 5	n = 7	n = 9	n = 11	n = 13	n = 15
9–18	K1	1.31	1.71	2.06	2.26	2.41	2.73
28–34	S1	1.04	1.06	1.09	1.19	1.33	1.50
40–45	H1	1.74	1.83	1.94	2.23	2.63	3.05
54–67	H2	1.63	1.62	1.92	2.13	2.43	2.79
72–81	K2A	1.29	1.53	1.72	2.07	2.57	3.28
84–91	K2B	1.29	1.60	2.08	2.64	3.08	3.46
72–91	K2	1.27	1.53	1.82	2.24	2.67	3.19
92–98	S2	1.01	1.07	1.15	1.28	1.43	1.65
116–120	H3	1.63	1.57	2.00	3.04	3.79	4.68

Table 2

$\langle\beta_i\rangle$ for stages n=5 to n=15

Segment	Region	n = 5	n = 7	n = 9	n = 11	n = 13	n = 15
9–18	K1	1.62	1.83	1.99	1.98	1.84	1.61
28–34	S1	1.90	2.85	3.80	4.65	5.29	5.80
40–45	H1	1.19	1.54	2.03	2.33	2.35	2.27
54–67	H2	1.50	2.20	2.68	3.13	3.60	3.85
72–81	K2A	1.63	2.28	2.98	3.44	3.82	4.10
84–91	K2B	1.66	2.04	2.14	2.08	1.85	1.63
72–91	K2	1.68	2.19	2.56	2.77	2.82	2.80
92–98	S2	1.95	2.86	3.64	4.16	4.48	4.57
116–120	H3	1.57	2.33	2.51	2.06	1.44	0.85

Table 3

$\langle\Delta_i\rangle$ for stages n=5 to n=15

Segment	Region	n = 5	n = 7	n = 9	n = 11	n = 13	n = 15
9–18	K1	1.02	1.03	0.65	0.38	0.36	0.53
28–34	S1	0.91	0.82	0.68	0.58	0.46	0.39
40–45	H1	1.74	1.34	0.94	0.77	0.72	0.37
54–67	H2	1.13	0.71	0.82	0.72	0.50	0.13
72–81	K2A	0.92	0.63	0.45	0.13	0.10	−0.11
84–91	K2B	2.55	3.56	3.93	4.61	4.76	5.06
72–91	K2	1.73	1.38	1.12	0.97	1.13	0.96
92–98	S2	0.94	0.85	0.76	0.75	0.79	0.82
116–120	H3	3.44	1.71	3.30	4.36	7.14	10.0

Table 4

$\langle T_i \rangle$ for stages n=5 to n=15.

Segment	Region	n = 5	n = 7	n = 9	n = 11	n = 13	n = 15
9–18	K1 (τ_L)	0.268	0.654	0.998	1.324	1.439	1.600
	K1 (τ_R)	0.313	0.578	0.394	0.420	0.645	1.094
	K1 (T)	(0.86)	(1.13)	(2.53)	(3.15)	(2.23)	(1.46)
28–34	S1 (τ_L)	0.098	0.385	0.725	1.027	1.380	1.768
	S1 (τ_R)	0.029	0.126	0.308	0.576	1.228	2.035
	S1 (T)	(3.43)	(3.06)	(2.35)	(1.78)	(1.12)	(0.87)
40–45	H1 (τ_L)	0.767	0.784	0.912	1.053	0.870	0.704
	H1 (τ_R)	0.603	0.366	0.295	0.349	0.310	0.992
	H1 (T)	(1.27)	(2.14)	(3.09)	(3.02)	(1.43)	(0.71)
54–67	H2 (τ_L)	0.664	0.632	0.821	0.944	1.106	1.363
	H2 (τ_R)	0.673	0.773	1.294	1.578	1.796	2.204
	H2 (T)	(0.99)	(0.82)	(0.63)	(0.60)	(0.62)	(0.67)
72–81	K2A (τ_L)	0.369	0.802	1.362	1.858	2.112	2.429
	K2A (τ_R)	0.220	0.417	0.604	0.856	1.211	1.741
	K2A (T)	(1.68)	(1.92)	(2.26)	(2.17)	(1.74)	(1.39)
84–91	K2B (τ_L)	0.225	0.279	0.413	0.665	1.212	2.208
	K2B (τ_R)	0.266	0.575	0.990	1.261	1.004	0.861
	K2B (T)	(0.84)	(0.49)	(0.42)	(0.52)	(1.21)	(2.56)
72–91	K2 (τ_L)	0.291	0.571	0.932	1.357	1.731	2.243
	K2 (τ_R)	0.226	0.448	0.742	1.106	1.410	1.675
	K2 (T)	(0.84)	(1.27)	(1.25)	(1.23)	(1.23)	(1.34)
92–98	S2 (τ_L)	0.102	0.490	1.125	1.890	2.410	2.693
	S2 (τ_R)	0.125	0.197	0.283	0.525	0.909	1.390
	S2 (T)	(0.82)	(2.49)	(3.96)	(3.60)	(2.64)	(1.94)
116–120	H3 (τ_L)	0.451	1.018	1.204	0.704	0.292	0.708
	H3 (τ_R)	0.538	0.352	0.260	0.284	0.224	----
	H3 (T)	(0.84)	(2.89)	(4.63)	(2.48)	(1.30)	----